EPJ Web of Conferences will be set by the publisher
DOI: will be set by the publisher
© Owned by the authors, published by EDP Sciences, 2015

arXiv:1511.01936v1 [nucl-th] 5 Nov 2015

A new approach to barrier-top fission dynamics

G.F. Bertsch[a] and J.M. Mehlhaff

[1] *Department of Physics and Institute for Nuclear Theory, University of Washington, Seattle, WA USA*

Abstract. We proposed a calculational framework for describing induced fission that avoids the Bohr-Wheeler assumption of well-defined fission channels. The building blocks of our approach are configurations that form a discrete, orthogonal basis and can be characterized by both energy and shape. The dynamics is to be determined by interaction matrix elements between the states rather than by a Hill-Wheeler construction of a collective coordinate. Within our approach, several simple limits can be seen: diffusion; quantized conductance; and ordinary decay through channels. The specific proposal for the discrete basis is to use the K^π quantum numbers of the axially symmetric Hartree-Fock approximation to generate the configurations. Fission paths would be determined by hopping from configuration to configuration via the residual interaction. We show as an example the configurations needed to describe a fictitious fission decay $^{32}\mathrm{S} \rightarrow ^{16}\mathrm{O} + ^{16}\mathrm{O}$. We also examine the geometry of the path for fission of ^{236}U, measuring distances by the number of jumps needed to go to a new K^π partition.

1 Introduction

In this talk we will advocate a radically different approach to the theory of induced fission. To put this into context, we show in Fig. 1 a schematic view of the fission landscape with the different energy regions indicated by color. In the tunneling region, shown in green, the dynamics is driven by the pairing interaction. High above the barrier, shown in pink, we expect the dynamics to be highly overdamped and amenable to treatment by a diffusion equation. In between is the barrier-top region, shown in blue. This commonly described by the Bohr-Wheeler theory and its generalization to multiple barriers.

We seek an alternate treatment that does not require well-behaved channels to cross the barrier. The concept of a channel demands that the wave function can be written as a product of an internal part and a one-dimensional function of some collective coordinates. This is leads to the Born-Oppenheimer approximation in molecular dynamics, which is well justified by the large separation of electron and nucleus mass scales. But this not at all the case in nuclear physics, where both single-particle and collective structures are on the same 1 MeV energy scale. The tools for microscopic calculations in that framework are just not up to the task.

The present state of the art for modeling induced fission may be seen in the recent calculations of the Los Alamos group [1, 2]. The basic calculational framework was laid out by Bjørnholm and Lynn

[a] e-mail: bertsch@uw.edu

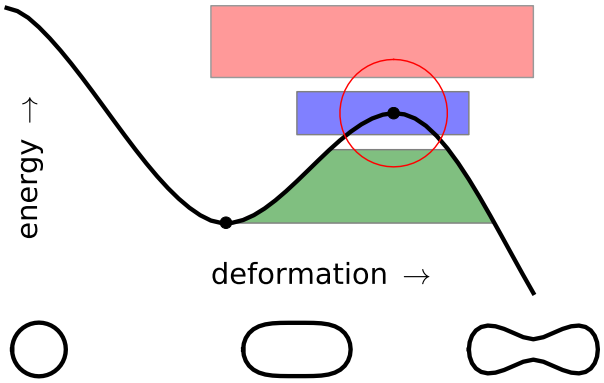

Figure 1. Schematic view of the fission landscape with a simple barrier. The colored regions show the areas of different dynamics: diffusive in pink, tunneling in green, and barrier-top in blue.

[3], who generalized the Bohr-Wheeler theory to deal with a fission landscape having two barriers. The degrees of freedom are depicted in Fig. 2. They are the state densities in wells I and II, indicated by dots in the Figure, and the channels at barriers A and B, indicated by the horizontal lines. The final formula for the fission decay rate is a generalization of the Bohr-Wheeler decay rate formula

$$W = \frac{1}{2\pi\hbar\rho} \sum_c T_c \tag{1}$$

which only has only one compound nucleus density ρ and only transmission coefficients T_c for a single barrier.

To connect this to a microscopic theory based on a nucleonic Hamiltonian, we need to know how to calculate the transmission coefficients T_c between states and channels, and also how calculate mixing between channels. The microscopic framework used up to now is the Generator Coordinate Method (GCM). Unfortunately, it does not have a natural place for the ordinary states and the needed connection to channels seems difficult to incorporate. For the mixing of channels, there is a heroic attempt by Gogny's group to set up a GCM framework for this purpose [5], but it appears to us to be very complicated to carry out in practice.

In our view, the problem is the channel picture itself. Channels are useful if there is clear separation between collective and intrinsic degrees of freedom. That is O.K. for the Born-Oppenheimer framework for molecular physics, but the separation of collective and intrinsic energy scales is simply not present in nuclear physics. Another problem is the non-orthogonality of the channel wave functions in the GCM. In particular, the over-completeness of the basis often gives rise numerical stabilities that can only be suppressed by ad hoc truncations.

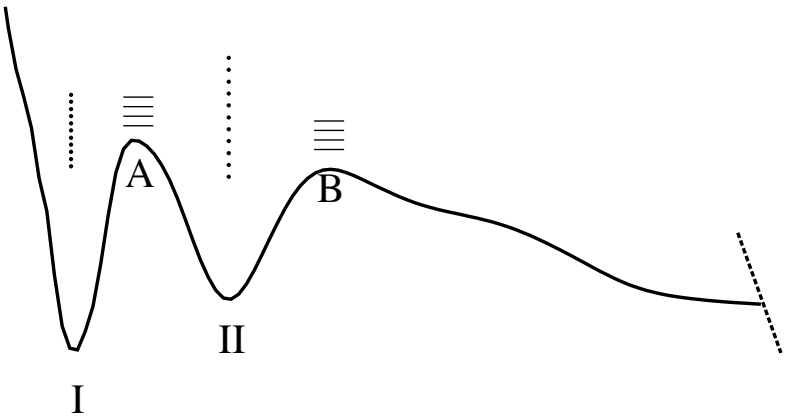

Figure 2. Fission potential energy surface (PES) for ^{236}U, taken from Fig. 7 of Ref. [4]. Dashed line shows energy of separated fission fragments at the same quadrupole deformation coordinate. Superimposed on the PES are the elements needed for the generalized Bohr-Wheeler description of the dynamics. Type I and II state are indicated by dots; channels bridging the barriers are indicated by horizontal lines. In practice, the channels are only needed at the barrier tops.

From the phenomenological side, the dynamics of induced fission may be much closer to a diffusive limit than an inertial limit. One sees from many studies including one presented in this Workshop [6] and a recent one on mass distributions [7] that statistical and diffusive models can describe many features of the fission final state. Furthermore, we also heard in the Workshop a report on a microscopic dynamical model that produced a fission time so large that inertial motion would be highly over-damped [8].

2 Dynamics in a discrete basis

There is an alternative. That is to construct a discrete basis for the Hamiltonian, avoiding completely the introduction of continuous collective degrees of freedom. In this section we show how various limits of the dynamics can emerge, deferring to the next section how we envisage constructing the basis. The basis will be composed of mean-field configurations, allowing one to calculate with well-known methods the matrix elements of Hamiltonians of the usual microscopic form,

$$H = \sum \varepsilon_i a_i^\dagger a_i + \frac{1}{4} \sum v_{ij,kl} a_i^\dagger a_j^\dagger a_l a_k. \tag{2}$$

Besides the close connection to configuration-interaction (CI) computational methods that have been so successful with the nuclear shell model, the discrete-basis framework provides a conceptual bridge to quantum transport in condensed matter physics.

The states need to be characterized by energy and some measure of the shape; these may be determined by the expectation values of the Hamiltonian and some single-particle operator such as the

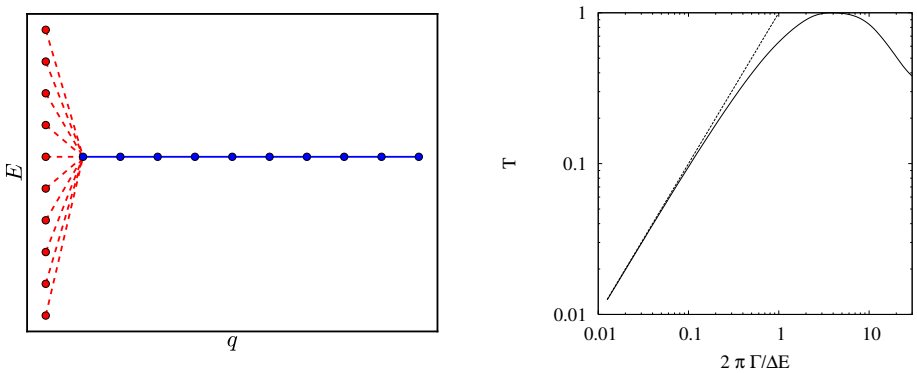

Figure 3. Discrete-state modeling of the compound nucleus coupling to a neutron decay channel. On the left are shown the states as circles and their couplings as lines. On the right is shown the calculated transmission coefficient T compared to the weak-absorption limit $T = 4\pi^2 v_c^2 \rho^2$.

quadrupole moment. It is then easy to set up conditions on Hamiltonian to realize different possibilities for the dynamics.

The first limit is that of a compound nucleus decaying into a single channel. The basis states are set up as shown in Fig. 3 on the left. The compound nucleus states are shown as the tower of states indicated as red points. The channel states are the regularly spaced blue point on the left. The interactions between the compound states and the first channel state are shown as the dashed red lines. They would be taken as Porter-Thomas distributed about some rms average value $\langle v_c^2 \rangle$. The interactions between channel states are shown as the solid blue lines. They would all be equal. Then the entire physics of scattering theory and compound nucleus resonances can be displayed by using standard methods. There has been recent interest in couplings to the continuum that violate Porter-Thomas statistics [9]; perhaps this model would be useful to explore such possibilities.

Another limit is one that approximates diffusive dynamics. By this we mean that wave packets decay according to the diffusion equation with some diffusion coefficient $D(q)$ according to the equation

$$\frac{\partial P}{\partial t} = \frac{\partial}{\partial q} D(q) \frac{\partial P}{\partial q} \tag{3}$$

where q is a shape index. To realize this limit in a discrete basis, we distribute the states in layers according to the shape parameter q and in energy according to Gaussian random matrix ensemble. The layout of states in the (E, q) plane is shown in Fig. 4 on the left. We also assume a Porter-Thomas distribution of interaction matrix elements, limited to states on next-neighbor layers. Evolving the dynamics by the time-dependent Schrödinger, we find probability distributions on the different layers at later times. The results are shown on the right-hand panel of the Figure at some fixed time. The points are an average of different Hamiltonians in the ensemble, with the error bars showing the r.m.s. fluctuations. The connection to macroscopic theory comes if we can relate the statistical properties of the Hamiltonian ensemble to a diffusion coefficent. This is given by the formula [10]

$$D = 2\pi\rho(E)\overline{(q_\alpha - q_\beta)^2 \langle \alpha | v | \beta \rangle^2} \tag{4}$$

where ρ is the level density in a single layer and the bar indicates an average over interactions between states in different layers. The red curve is the corresponding distribution predicted by the diffusion

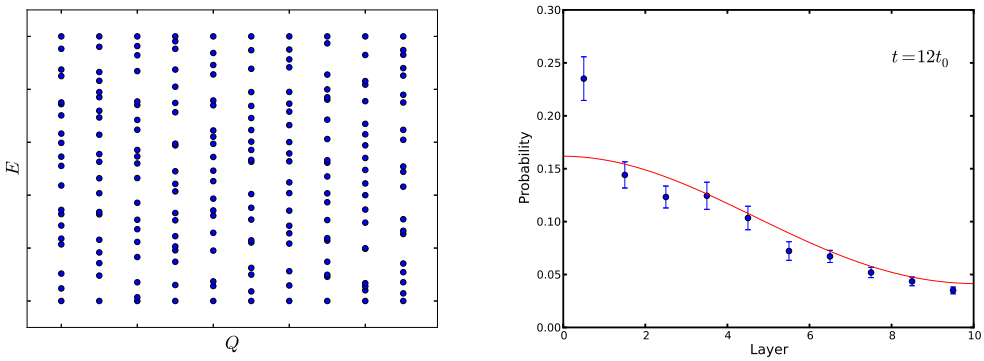

Figure 4. Discrete basis modeling of shape diffusion in a region of high level density. The states are grouped in vertical layers by their deformation, and it is assumed that only nearby layers are coupled by the interaction. The right hand side shown the probability distribution after some time interval, starting from an initial wave function localized on the first layer.

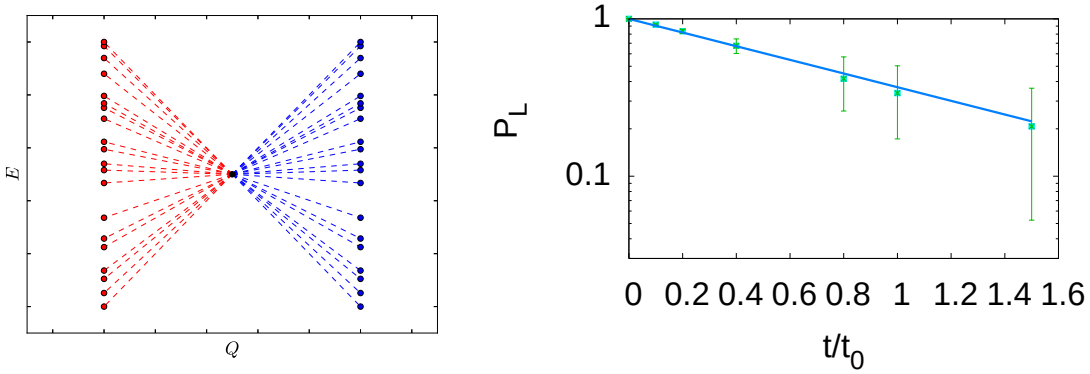

Figure 5. Discrete state representation of resonance-mediated conductances. The states of the compound nucleus are on the left, and the post-barrier states are on the right.

equation, the D from Eq. (4). One sees that the classical physics is quite accurate except for the some trapping in first layer.

Another interesting limit is what may be called resonance-mediated conductance. It is inspired as a very simplified model for fission dynamics at the barrier top as well as for the conduction of electrons from one conductor to another through a quantum dot. The layout of states is shown in Fig. 5. The transport takes place through the single state in the middle. There is a lot of physics that can be explored with this model [11]. For this talk, we just mention one limit. With suitable restrictions on level densities and interaction strengths, the rate at which the system goes from one side to the other

Table 1. Orbital filling for ^{16}O in the spherical shell model. The columns separate the K quantum number, and the rows separate nucleon type and parity.

K	1/2	3/2	5/2
p^+	2	0	0
p^-	4	2	0
n^+	2	0	0
n^-	4	2	0

can be calculated by Eq. (1) with the transmission coefficient given by the formula [12]

$$T_r = \frac{\Gamma_R \Gamma_L}{E_b^2 + (\Gamma_R + \Gamma_L)^2/4}. \tag{5}$$

Here the decay widths of the resonance to the left and to the right (Γ_L and Γ_R) are calculated by Fermi's Golden Rule. Again, we examine an ensemble of Hamiltonians using random matrix energy spacings, but now with fixed couplings to the resonance to satisfy Eq. (5) with $T_r = 1$. The resulting time-dependent probability for staying on the left is shown in the panel on the right, with error bars showing the fluctuations in the ensemble. The solid line is an exponential decay with the decay rate determined by Eq. (1) with the calculated transmission factor. We see that the average decay rate is well reproduced, but there is considerable fluctuation due to the level-density fluctuations in the random-matrix ensemble.

3 An implementation: the axial basis

A discrete basis should be composed of orthogonal states, and it should be extendible in principle to a complete basis. A good candidate to satisfy these requirements is what we shall call the axial basis. As in traditional theory, the underlying framework is self-consistent mean-field theory. But instead of adding a generator-coordinate field to distinguish states, we use the partition of the particle numbers to orbitals of different K quantum numbers to make a first landscape of the PES. To make this clear, let us consider a very simple example, the shell-model ground state of ^{16}O. The filled shells are $s_{1/2}, p_{3/2}, p_{1/2}$. The K quantum number can be taken as the azimuthal angular momenta j_z of the shells. This produce the fillings shown in Table I, amounting to a partition of the 16 nucleus into 6 K^π sets.

To see how the scheme might work, we examine the partitions for a toy model, the fission of ^{32}S into two ^{16}O nuclei with a Hamiltonian tuned to allow the decay. This model was proposed in Ref. [13]. Tables of the partitions are shown in Fig. 6. The leftmost table gives the K^π partition for ^{32}S as a spherical shell-model configuration. The filled shells are $0s_{1/2}, p_{3/2}, p_{1/2}, d_{5/2}, 1s_{1/2}$. Notice that the nonzero K^π orbitals go up to the $5/2^+$ associated with the $d_{5/2}$ shell. The partition table for ^{16}O+^{16}O can be constructed by a very simple argument. The orbitals of the combined system have the same K quantum numbers as the individual nuclei if the fission is along the z-axis. Each orbital has an extra two-fold degeneracy because of its presence in both O nuclei. The plus and minus linear combinations will have good parity. Thus, each orbital in the individual O gives rise to two orbitals with the same K but opposite parities in the combined system. The resulting partitions are shown on the right hand side of the Figure. Comparing the initial and final partitions, one sees that the decay requires four particles to be moved from $K^\pi = 5/2^+$ orbitals to $K^\pi = 1/2^-$ orbitals. The various configurations involved in the decay are depicted in the energy-versus-shape graph in the bottom panel of the figure. On the left is the ^{32}S ground state. The residual interaction connects it (dotted line) with

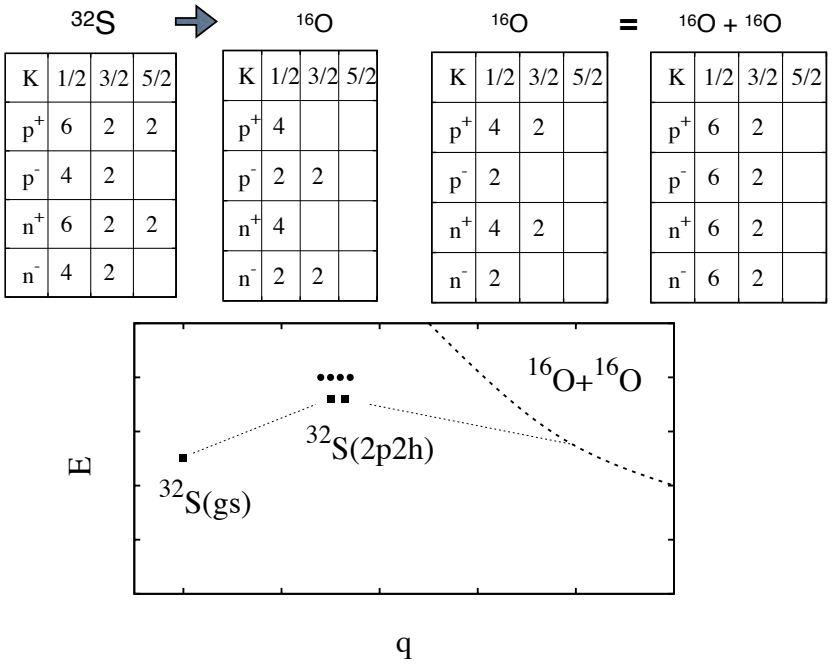

Figure 6. Fission of ^{32}S in a toy model. See text for explanation.

several 2-particle 2-hole states as depicted in the middle. Finally, a second application of the residual interaction connects the intermediate configurations to the final partition. We have indicated the last configuration with a dashed line because it is not clear whether it would have a stable minimum in the Hartree-Fock minimization. It might be that the energy decreases continuously as the distance between centers increases. At that point we cannot avoid dealing with the problem of coupling to the continuum.

The next example exhibits the first steps to building a basis for treating the dynamics in the configuration-interaction framework. We start with a specific Hamiltonian of the usual shell-model form Eq. (2). The goal is to examine all possible partitions and determine the self-consistent minimum of each one. These states will span the range of deformations permitted by the shell-model space. Additional excited states in the same partitions may be constructed as particle-hole excitations with the same mean field as the ground state in that partitions. We have written a code to carry out the fixed-partition ground state minimization, given H of the form Eq. (2). The example we show is the nucleus ^{162}Dy, see Fig. 7. Here we took a Hamiltonian constructed for use in the Shell Model Monte Carlo treatment of level densities [14]. The filled circle shows the ground state of the axial Hartree-Fock approximation. This state is moderately deformed, as is expected for midrange lanthanide nuclei. The open circles show the lowest excited states that arise by changing the partition by a single pair jump. One see a significant gap in the spectrum, and also that the quadrupole deformations are not very different from that of the ground state. The partial localization in deformation is important to obtain eventually a collective dynamics for a deformation coordinate.

Now we come to the actinide nuclei and realistic fission paths. We start with the two ground states I and II in the PES minima. Fig. 8 shows the difference in the partitions of the two states, as

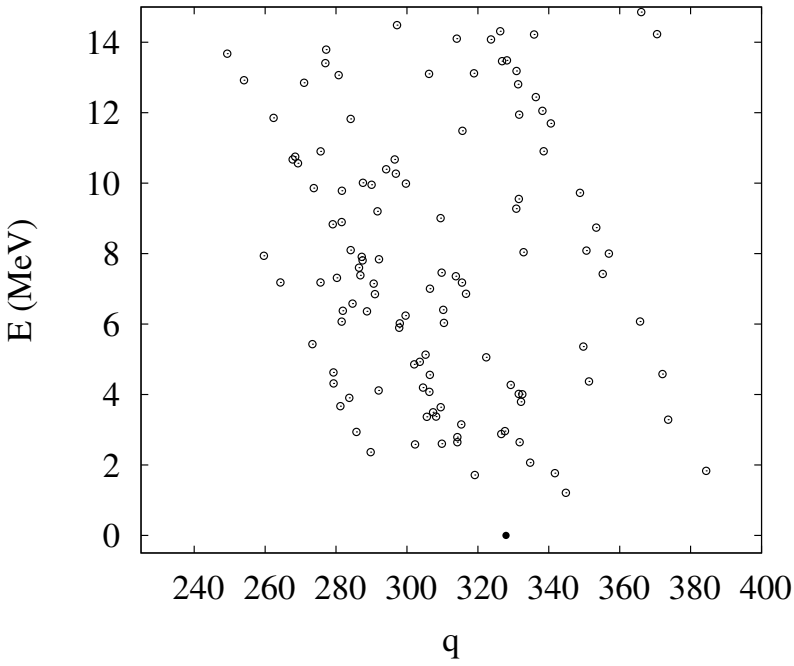

Figure 7. Ground state configuration of ^{162}Dy (filled circle) and excitded state configurations reachable by a single pair jump (open circles).

calculated by Möller in the FRLD model [15, 19]. One sees that particles in higher-K orbitals are moved to lower K in going from the first minimum to the second. The number of pairs to be moved totals 6. To explore the partition space between the two minima, we should have a self-consistent mean field code that allows one to specify the partition, with no other constraints. Lacking that, we can begin to map the distance between configurations with existing codes, using the jump number as the distance measure. We did this for ^{236}U using the HFBaxial code written by Luis Robledo [16]. The configurations we examined are the I and II ground states, the A and B barriers, and a number of configurations beyond the second barrier up to Q = 140 bn. At the largest deformation, the separated fragments have the same energy as the elongated fissioning nucleus. The results are shown in Fig. 9. First note that the shortest path from the I ground state to II is not over the saddle. Past the second saddle, the configurations are labeled by their quadrupole moment. In this region, the system is asymmetric and parity is not a good quantum quantum number. However, for the figure we have reported jump numbers corresponding to symmetric fission. It will be interesting to see the effect on the jump numbers when the parity constraint is released. If they remain substantial, it shows that the saddle-to-scission path requires dynamics beyond that contained in the time-dependent Hartree-Fock approximation.

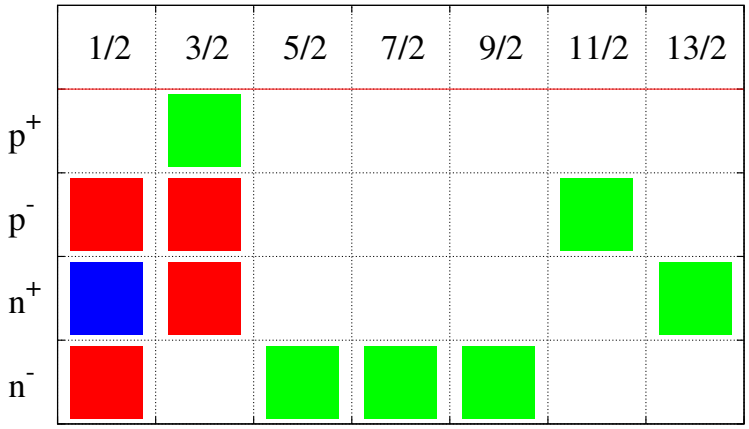

Figure 8. Difference of partitions in ^{236}U for the class I and class II ground states in the FRLD model [19].

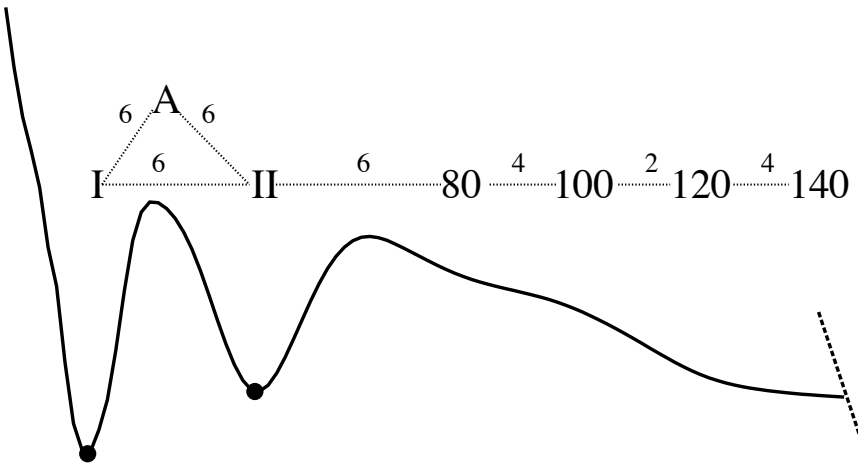

Figure 9. Schematic view of the fission barrier as in Fig. 2. The states I,II,A and B are unconstrained while the states by a quadrupole moment $Q = 80, 100, 120, 140$ are constrained by that operator. The distance between states is shown by the number of pair jumps to get from one to another.

4 The Hamiltonian

While there are many energy density functionals available for self-consistent mean-field theory, there does not yet exist a fully self-consistent effective Hamiltonian for nuclear structure. Still, it should be useful to explore the dynamics that follow from simplified residual interactions.

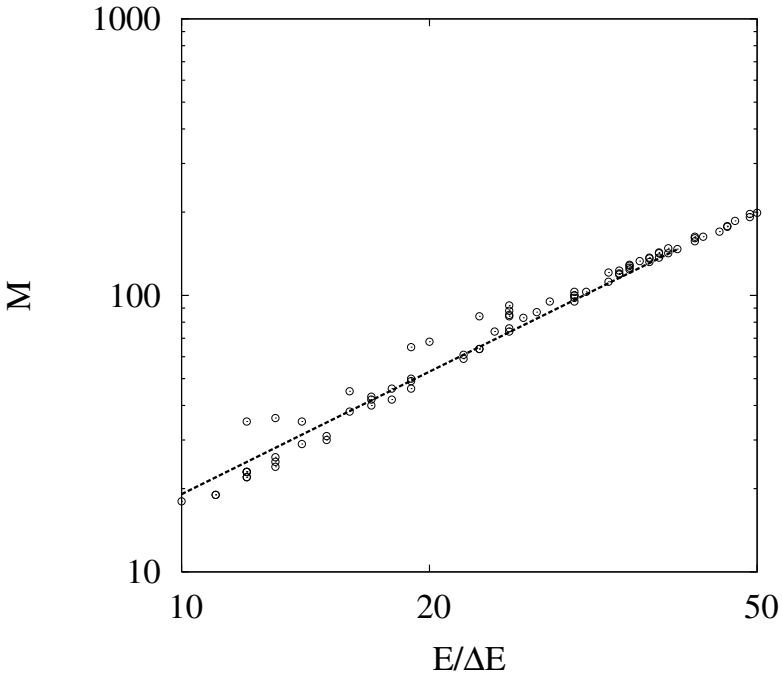

Figure 10. Relative interaction strengths to mix configurations at the same energy, as a function of excitation energy. See text for explanation.

4.1 Interaction between configurations

The two-particle interaction between configurations can be written schematically as

$$\langle\alpha|v|\beta\rangle = \sum \langle pp|v|pp\rangle \det|\langle\phi_i^\alpha|\phi_j^\beta\rangle| \tag{6}$$

where $\langle pp|v|pp\rangle$ is a two-body matrix element and $\det|\langle\phi_i^\alpha|\phi_j^\beta\rangle|$ is the overlap of spectator orbitals.

From the study of the dynamics as seen for example in Fig. 4, it is clear that an important parameter to approach the diffusion limit is the ratio of the mean-square average of the interaction between configurations $\overline{\langle i|v|j\rangle^2}$ to the local level density $\rho(q)$. If this ratio is large, each state decays exponentially into nearby states and the dynamics will be diffusive. It has been shown in a simple model that this ratio increases with excitation energy [10], so the diffusion limit will be appropriate at high enough excitation energy. In that model, the average interaction strength scaled with excitation energy E as

$$\overline{\langle\alpha|v|\beta\rangle^2} \sim E^{3/2}/\rho(E). \tag{7}$$

We also have analyzed this with a somewhat more sophisticated model, with results shown in Fig. 10. The vertical scale is proportional to the product $\overline{\langle\alpha|v|\beta\rangle^2}\rho(E)$. It is plotted with respect to excitation energy, measured in units of the single-particle energy spacing. The dotted line is a power-law fit to the ratios; it comes out very close to the predicted 3/2-power dependence. Details will be given elsewhere.

The matrix elements of the two-body interaction are also affected by the changes in the spectator orbitals due to the different mean fields of the partitions. This cuts down the interactions by the determinant of spectator orbital overlaps indicated in Eq. 6. This is a good occasion to mention the early paper by Arima and Yoshida giving analytic expressions for this determinant in the harmonic oscillator basis [17].

So where do we hope to go from here? It seems feasible in the near term to go beyond simple models to sample the CI interactions arising from realistic effective Hamiltonians. We can then use the derived statistical properties to determine where the diffusive limit can be applied.

5 Acknowledgments

We wish to thank A. Bulgac for discussions, L. Robledo for the use of the HFBaxial code to calculate partitions of ^{236}U, and P. Möller for providing us with the orbital fillings for ^{236}U in the FRLD model. We also acknowledge financial support from the Institute for Nuclear Theory (GFB) and from the DOE under Grant FG02-00ER41132 (JMM).

References

[1] O. Bouland, J.E. Lynn, and P. Talou, Phys. Rev. C **88** 054612 (2013).
[2] O. Bouland, J.E. Lynn, and P. Talou, Nucl. Data Sheets **118** 211 (2014).
[3] S. Bjørnholm and J.E. Lynn, Rev. Mod. Phys. **52** 725 (1980).
[4] R. Rodriguez-Guzman and L.M. Robledo, Phys. Rev. C **89** 054310 (2014).
[5] R. Bernard, H. Goutte, D. Gogny and W. Younes, Phys. Rev. C **84** 044308 (2011)
[6] J.-L. Sida, contribution to this workshop and J.-F. Lemaître, et al., Phys. Rev. C **92** 034617 (2015).
[7] J. Randrup and P. Möller, Phys. Rev. Lett. **106** 132503 (2011).
[8] A. Bulgac, contribution to this workshop.
[9] S. Mizutori, contribution to this workshop.
[10] B.W. Bush, G.F. Bertsch, and B.A. Brown, Phys. Rev. Lett. C **45** 1709. (1992).
[11] G.F. Bertsch, arXiv:1407.1899.pdf (2014).
[12] Y. Alhassid, Rev. Mod. Phys. **72** 895 (2000).
[13] J.W. Negele, Nucl. Phys. A **502** 371 (1989).
[14] Y. Alhassid, L. Fang and H. Nakada, Phys. Rev. Lett. **101** 082501 (2008).
[15] P. Möller, et al., Atomic Data and Nuclear Data Tables **59** 185 (1995).
[16] L.M. Robledo, private communication. See also Ref. [18].
[17] A. Arima and S. Yoshida, Nucl Phys. **12** 139 (1959).
[18] M. Warda, J.L. Egido, L.M. Robledo, and K. Pomorski, Phys. Rev. C **66**, 014310 (2002).
[19] P. Möller, private communication.